Flux-flow resistance in the cuprate superconductor $Nd_{2-x}Ce_xCuO_y$: Spatial domains and spontaneous oscillations

A. Wehner,[1] O. M. Stoll,[1] R. P. Huebener,[1] and M. Naito[2]
[1]*Physikalisches Institut, Lehrstuhl Experimentalphysik II, Universität Tübingen, Morgenstelle 14, D-72076 Tübingen, Germany*
[2]*NTT Basic Research Laboratories, 3-1 Morinosato-Wakamiya, Atsugi-shi, Kanagawa, 243-01, Japan*
(Received 18 October 2000; published 19 March 2001)

Under quasi-voltage-bias, time-averaged measurements in epitaxial *c*-axis-oriented films of $Nd_{2-x}Ce_xCuO_y$ (NCCO) show the nucleation and growth of a high-electric-field domain. Time-resolved resistance measurements indicate spontaneous oscillations, apparently due to a breathing movement of the domain boundary. During the experiments the samples were immersed in superfluid helium at 1.92 K. The observed nonlinear phenomena suggest a strong electric-field dependence of the quasiparticle scattering rate. Since the symmetry of the pair wave function affects the electronic structure of the quasiparticle system, the correct symmetry in NCCO represents a crucial input of a model for explaining these observations.

DOI: 10.1103/PhysRevB.63.144511 PACS number(s): 74.25.Fy, 74.60.Ge, 74.72.Jt

I. INTRODUCTION

Recently, we have reported the observation of an intrinsic hysteretic step structure of the flux-flow resistance under current bias in epitaxial *c*-axis oriented films of the cuprate superconductor $Nd_{2-x}Ce_xCuO_y$ (NCCO) at intermediate magnetic fields $B_{c1} \ll B < B_{c2}$.[1] Under quasi-voltage bias, negative differential resistance (NDR) and spontaneous resistance oscillations were found.[2,3] During measurements, the samples were imbedded in liquid helium, mostly in superfluid helium, i.e., at $T < 2.17$ K. The underlying instability appears to be due to a characteristic electric-field dependence of the flux-flow resistance resulting from the electronic structure of the vortex system in the mixed state.[4] NCCO is an electron-doped superconductor. For some time the experimental evidence indicated an *s*-wave symmetry of the pair wave function in NCCO.[5–10] However, recently evidence of *d*-wave symmetry has also been reported, including a detailed discussion of this symmetry issue.[11,12] Clearly, the symmetry of the pair wave function plays a crucial role in the development of a model for explaining the observed instabilities of the flux-flow resistance of NCCO.

In our previous discussion[3,13–15] we proposed a model based on the existence of two narrow subbands between the Fermi energy and the gap energy. These subbands develop from Andreev bound states in the core of an isolated vortex, if the vortex interaction becomes important and the bound-state wave functions of two neighboring vortices overlap. In an electric field generated by vortex motion, the quasiparticles in the narrow subbands can be shifted energetically up to the band edge, such that Bragg reflection and Bloch oscillations occur. This mechanism for generating the instabilities and NDR in NCCO appears to be favorable if the pair wave function shows an *s*-wave symmetry.

In a more general second model, instead of the subband structure we have assumed that in the quasiparticle density of states (DOS) steps appear as a function of energy between the Fermi energy and the gap energy.[1,4,16] Since the DOS provides the phase space available for quasiparticle scattering, the electric-field-induced quasiparticle energy shift leads to a field dependence of the electric resistance and, hence, to the observed nonlinear behavior. This second model appears attractive in the *d*-wave case. Since this model is more general, and since *d*-wave symmetry now appears likely in NCCO,[11,12] we concentrate our discussion on the second model.

In this paper we report on spatially and temporally resolved flux-flow resistance measurements in NCCO films performed under quasi-voltage bias. Spatial discrimination was achieved by placing a series of voltage leads along the sample. In this way the nucleation and growth of a high-electric-field domain was observed. In addition, in the NDR regime we observed spontaneous flux-flow resistance oscillations which apparently are due to a breathing movement of the domain boundary.

II. SAMPLES AND EXPERIMENTAL TECHNIQUES

Details of the experimental techniques are described in Refs. 1 and 3. In the following we summarize the essential points. The samples were epitaxial *c*-axis-oriented films of the cuprate superconductor $Nd_{2-x}Ce_xCuO_y$ close to optimum doping ($x = 0.15$). The different samples had a critical temperature in the range $T_c = 23.4 - 24.0$ K with a transition width of typically $\delta T_c = 0.6 - 0.8$ K. At 30 K the electric resistivity values were in the range $\rho(30\,\mathrm{K}) = 20.2 - 26.3\ \mu\Omega$ cm. The thin-film bridges had the following geometry: width $w = 40\ \mu$m and thickness $d = 90 - 100$ nm. Four voltage leads were placed along the bridges as shown in the inset of Fig. 3. The inner distance between two neighboring leads was $L_i = 100\ \mu$m, and between the two outer leads $L_o = 360\ \mu$m. The current leads were attached further outside the outer voltage leads. During the flux-flow resistance measurements the samples were immersed in superfluid helium (in order to minimize the influence of Joule heating) kept at the temperature $T = 1.92$ K. A superconducting magnet served for applying a magnetic field parallel to the *c* axis of the films.

In addition to current-biased measurements, the dominant part of the experiments was performed using quasi-voltage bias, as described in Ref. 3. For clarity, the circuit of the

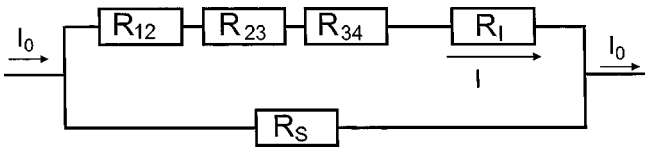

FIG. 1. Circuit for the quasi-voltage-biased measurements. Further details are given in the text.

latter measurements is shown schematically in Fig. 1. The sample is indicated by the three resistors R_{12}, R_{23}, and R_{34}, representing the three sections defined by the four voltage leads (see the inset of Fig. 3). The resistance $R_I = 100-300\,\mathrm{m}\Omega$ in series with the sample yields the sample current I by detecting the voltage drop along R_I. The shunt resistance $R_S = 1-3\ \Omega$ provides the quasi-voltage bias of the sample. R_I is placed in the liquid helium together with the sample. R_S is located outside the liquid helium, since it must carry electric currents up to 2 Å.

III. SPATIALLY RESOLVED MEASUREMENTS: GROWTH OF A HIGH-ELECTRIC-FIELD DOMAIN

A typical series of voltage-current characteristics (VIC's) measured at 1.92 K and different magnetic fields is shown in Fig. 2. From right to left the magnetic field increases from 1000 to 3000 mT in 400-mT steps. The sample geometry is indicated in the inset of Fig. 3. The voltage plotted in Fig. 2 is the total voltage between the outer voltage leads, i.e., the sum of the voltages of the three sample sections: $V = V_{12} + V_{23} + V_{34}$ (plus a small contribution from the sample sections occupied by the two inner voltage leads). The black curves refer to current-biased measurements for increasing current, whereas the gray curves were measured using quasi-voltage bias for increasing voltage. Whereas a large flux-flow resistance step appears in the curves for current bias, in the voltage-biased curves this step is replaced by a branch of

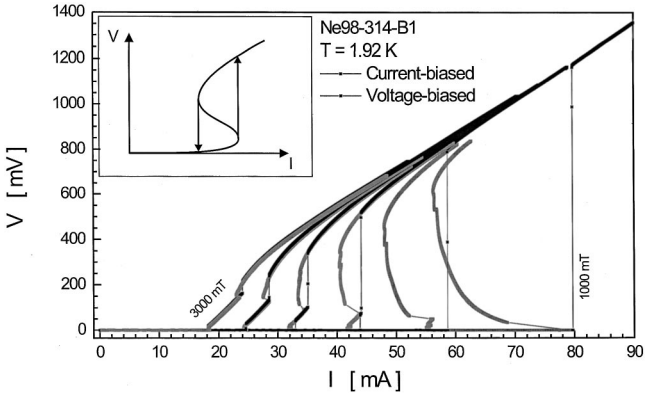

FIG. 2. Typical VIC's at $T = 1.92$ K. From right to left the magnetic field increases from 1000 to 3000 mT in 400 mT steps. The plotted voltage is the sum of the voltages of the three sample sections: $V = V_{12} + V_{23} + V_{34}$ (plus a small contribution from the sample sections occupied by the two inner voltage leads). Black curves: current bias with increasing current. Gray curves: quasi-voltage-bias for increasing voltage. The inset shows, schematically, the hysteresis of the current-biased measurements.

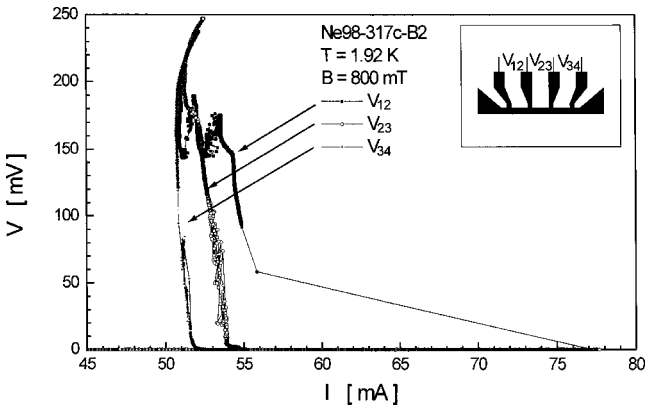

FIG. 3. Spatially resolved voltage measurements. VIC's of the three sample sections: V_{12} (solid square), V_{23} (open circle), and V_{34} (cross) vs current at $T = 1.92$ K and $B = 800$ mT. The inset shows the sample geometry.

NDR. The voltage steps of the current-biased curves originate exactly at the *lower* end of the NDR regions observed for quasi voltage bias. On the other hand, for *decreasing current* the voltage steps for current bias were found to start exactly at the *upper* end of the NDR regions. In this way the hysteretic step structure for current bias is established. For clarity the curves for decreasing current are not included in Fig. 2. However, the hysteretic behavior is indicated schematically in the inset. We emphasize that perfect voltage bias (with zero load resistance and a horizontal load line in Fig. 2) is impossible because of the small input impedance of the samples and the finite load resistance. Due to this limitation the NDR branch associated with the lower voltage step appearing at a much smaller onset voltage of about 15 μV (Ref. 1) could not be observed separately.

Next we turn to the spatially resolved flux-flow resistance measurements made possible with the sample geometry shown in the inset of Fig. 3. In the main part of this figure we show typical results for $T = 1.92$ K and $B = 800$ mT. The quasi-voltage bias was applied with the voltage increasing using the circuit displayed in Fig. 1. The nucleation of the high-electric-field domain is seen to start in section 12. In this section the VIC first displays the negative slope of the load line, and above about 50–70 mV it turns upward with a steeper negative slope. Up to the value $V_{12} \approx 150$ mV the voltages in the other two sample sections remain undetectable on this plot. (We will discuss the results obtained under much higher voltage resolution further below.) At $I \approx 54$ mA, section 23 shows the first appearance of resistance, leading to a kink in the $V_{12}(I)$ curve due to the overall voltage bias. In the current range below $I \approx 53.5$ mA the curve $V_{23}(I)$ develops a steep negative slope simultaneously with the appearance of a minimum of $V_{12}(I)$. Section 34 becomes resistive below about $I \approx 52$ mA. Simultaneously with the steep negative slope of $V_{34}(I)$, a second minimum in $V_{12}(I)$ and a kink in $V_{23}(I)$ appears. The detailed pattern of all three curves in Fig. 3 can be well understood from the overall voltage bias of the sum of the three voltages V_{12}, V_{23}, and V_{34}. The other important conclusion from the results shown in Fig. 3 is the fact that a *single high-electric-field domain* is

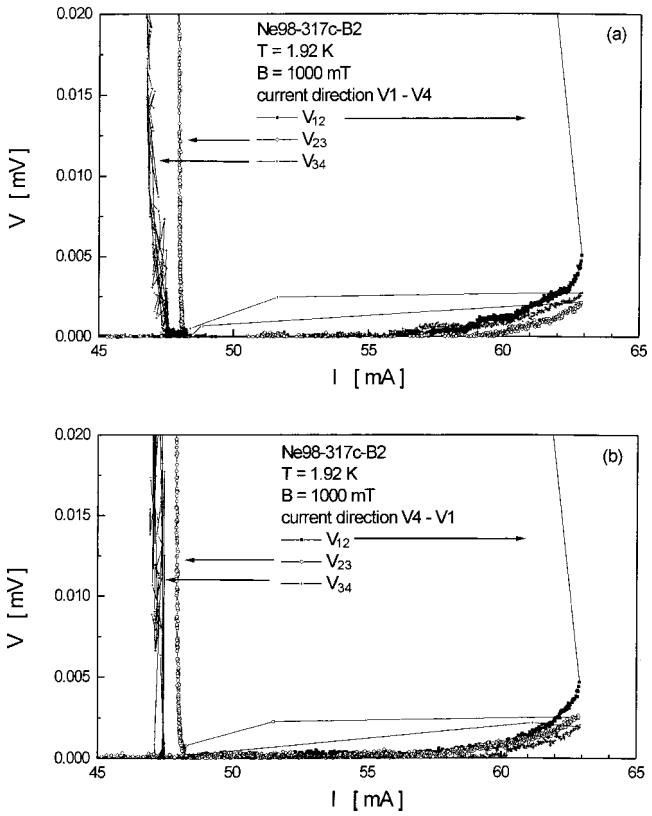

FIG. 4. Spatially resolved voltage measurements. V_{12} (solid square), V_{23} (open circle), and V_{34} (cross) vs current at $T=1.92\,\mathrm{K}$ and $B=1000\,\mathrm{mT}$. The voltage resolution is more than a factor 10^4 higher than in Fig. 3. (a) and (b) refer to opposite current direction.

nucleated initially in section 12 and subsequently grows to fill the next section and then the second to next section. Reversing the electric current kept the three voltages in Fig. 3 exactly the same. This apparently indicates that the domain nucleation site represents a sample inhomogeneity, and that the growth process of the domain in not affected by the current direction. In this context we note that, in principle, the nearly simultaneous nucleation of several or many high-electric-field domains in the three sample sections also may have been possible. However, such a scenario is clearly eliminated by our experiments.

From Fig. 3 we see that there exist two small current intervals where the data are relatively noisy and where the $V_{12}(I)$ curve turns over showing a positive slope. It appears likely that this noisy behavior is due to the spontaneous oscillations of the flux-flow resistance discussed in Sec. IV, and interpreted as a breathing movement of the domain boundary. The noisy current intervals in Fig. 3 coincide with the current region at which the growing high-electric-field domain just enters the next section of the sample. Hence the spontaneous current oscillations apparently lead to an increased noise level if the domain boundary is located near the border between two sample sections. We will return to this subject in Sec. IV.

Next we discuss the results obtained at much *higher voltage resolution*. In Fig. 4 we show the voltages V_{12}, V_{23}, and V_{34} of the three sample sections versus current at T

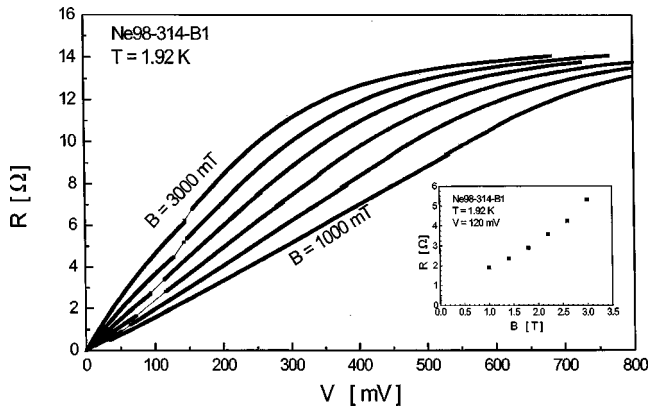

FIG. 5. Resistance $R=V/I$ calculated for the quasi-voltage-biased curves of Fig. 2 plotted vs the voltage. The inset shows R at $V=120\,\mathrm{mV}$ vs B.

$=1.92\,\mathrm{K}$ and $B=1000\,\mathrm{mT}$ for the same sample as in Fig. 3. The voltage resolution is now increased by a factor larger than 10^4 and, again, quasi-voltage bias is applied. In order to demonstrate the high reproducibility for opposite current directions, in Figs. 4(a) and 4(b), respectively, the results for both current directions are displayed separately. We see that the resistive behavior in the three sample sections is independent of the current direction. With increasing current the three sample sections show the onset of a resistive voltage at about the same current, and initially the three VIC's of the individual sections are quite similar. This behavior agrees exactly with our previous results obtained under current control.[1] At $V\approx 0.005\,\mathrm{mV}$ in section 12, a high-electric-field domain nucleates, and the voltage $V_{12}(I)$ increases rapidly with a steep negative slope. Due to the quasi-voltage bias the current decreases, and sections 23 and 34 return to the zero-voltage state. Only at a much higher voltage V_{12}, when the high-field domain enters section 23, does the voltage V_{23} increase rapidly. The same occurs again for section 34 and voltage V_{34}, when the high-electric-field domain enters section 34, and now we are back to our discussion of Fig. 3.

At $T=1.92\,\mathrm{K}$ we have performed quasi-voltage-biased measurements for two samples with the geometry shown in the inset of Fig. 3, at different magnetic fields in the range $B=600-1200\,\mathrm{mT}$. The results were qualitatively similar to those of Figs. 3 and 4.

As we have seen from our discussion of the results in Figs. 3 and 4, under quasi-voltage bias a high-electric-field domain is nucleated at one end of the sample, which subsequently grows until it extends over the total sample length. This domain growth is also clearly indicated if the resistance $R=V/I$ is calculated for the voltage biased curves in Fig. 2, and is plotted versus the voltage V. This plot is shown in Fig. 5. On the low-voltage end all curves turn into nearly straight lines passing through the origin. This is very consistent with the growth of a single high-electric-field domain from one end of the sample to the other. Initially the slope of the curves increases nearly in proportion to B, as also shown in the inset, where the resistance R at $V=120\,\mathrm{mV}$ is plotted versus B. On the high-voltage end all curves turn over approaching a common saturation value $R\approx 15\,\Omega$, which is

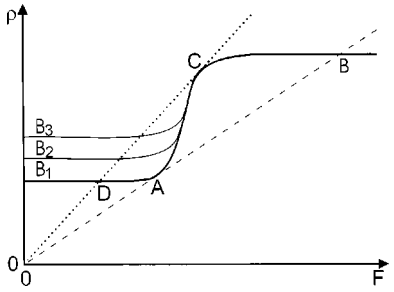

FIG. 6. Electric-field-dependent resistivity $\rho(F)$ yielding a nonlinear VIC displaying NDR and hysteresis. The different curve sections marked B_1, B_2, and B_3, respectively, schematically indicate the low-electric-field limit for increasing magnetic field ($B_1<B_2<B_3$).

identical to the normal resistance obtained from the plot in Fig. 2 for $I=90\,\mathrm{mA}$.

The high-electric-field domain indicated by our spatially resolved flux-flow resistance measurements apparently represents a sample region with a strongly increased flux-flow velocity. In principle, the necessary shearing of the vortex lattice at the location where the vortex velocity changes can occur within the distance of a single vortex lattice constant. This stationary appearance of the high-field domain in the mixed state of NCCO is distinctly different from the running behavior of the high-field domains due to the Gunn effect in semiconductors.

As we see from Fig. 2, the hysteresis of the VIC's strongly decreases with increasing magnetic field. This can be qualitatively understood from our earlier discussion of the underlying electric-field dependence of the flux-flow resistance.[4] Our argument is described schematically in Fig. 6, extending this earlier discussion. If the resistivity ρ displays the step structure as a function of the electric field F indicated by the solid line, under current bias for increasing current the resistivity jumps from point A to point B, and for decreasing current from point C to point D. Point A (point C) represents the value where the $\rho(F)$ curve is touched from below (above) by the dashed (dotted) straight line passing through the origin. Point B (point D) represents the crossing point of the dashed (dotted) straight line with the $\rho(F)$ curve. As we discussed in Refs. 1, 4, and 16, the step in the $\rho(F)$ dependence is likely to appear at the field F at which the quasiparticle energy is shifted from ϵ_F to $\epsilon_F\pm\Delta$ because of the nonequilibrium distribution in the field F (ϵ_F = Fermi energy; Δ is the superconducting energy gap). Near $\epsilon_F\pm\Delta$ the energy dependence of the quasiparticle DOS shows a distinct increase of the DOS with energy. Since the DOS provides the phase space available for scattering, the quasiparticle energy shift results in the electric-field dependence of the resistivity indicated schematically in Fig. 6. With increasing magnetic field the limiting resistivity values $\rho(F\rightarrow 0)$ are expected to increase, as indicated by the shifted horizontal curve sections marked B_1, B_2, and B_3, respectively, with $B_1<B_2<B_3$. Points $A-D$ have been constructed above based on curve section B_1. If this construction is repeated for sections B_2 and B_3, one sees immediately that with an increasing value of the limit $\rho(F\rightarrow 0)$ the magnitude of the step in the $\rho(F)$ dependence is reduced, point $B(D)$ moves to a lower (higher) electric field F, and the hysteresis of the VIC's strongly decreases. This is indicated exactly by the data of Fig. 2.

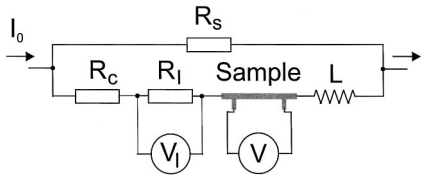

FIG. 7. Extended circuit of the quasi-voltage-biased measurements, including the inductance L and the contact resistance R_c. Further details are given in the text.

IV. SPONTANEOUS OSCILLATIONS OF THE FLUX-FLOW RESISTANCE

In Sec. III we dealt exclusively with *time-averaged* measurements. Next we turn to *time-resolved* experiments for observing spontaneous oscillations of the flux-flow resistance. The measuring circuit was the same as before. However, the voltages along the sample and along the resistance R_I were recorded using a storage oscilloscope. Further, various inductances L were inserted into the circuit. This extended circuit is shown schematically in Fig. 7. L represents the inductance given by the wiring and the various inductances added to the circuit. R_c denotes the resistance of the wiring which is given mostly by the contact resistance. In Fig. 7 only two voltage leads at the sample are shown for simplicity, although the four leads indicated in the inset of Fig. 3 were available for studying the three sections separately.

Keeping the dc operating point on the NDR branch of the VIC constant, we have observed two types of spontaneous flux-flow resistance oscillations, depending on the inductance L in the circuit. For the following results the magnetic field was kept at $B=1000\,\mathrm{mT}$ or below, where only a single large step or NDR branch appeared in the VIC's. In Fig. 8(a) we show typical current oscillations observed for small inductance values $L<L_{\min}$, with $L_{\min}=400\,\mu\mathrm{H}$. The frequencies were in the range $f=10-40\,\mathrm{kHz}$, decreasing with increasing dc voltage, as seen in Fig. 8(b). For $L<L_{\min}$ the frequency was independent of L, as indicated in the inset of Fig. 8(b). This type of oscillation was observed only at temperatures below 2.17 K, where the samples were imbedded in superfluid helium. In the following we refer to this type as *structure limited oscillations* (SLO's), since their temporal behavior appears to be dominated by the domain structure in the sample, in this way representing an intrinsic property.

The second type of oscillation was observed only if the inductance L in the circuit exceeded the value $L_{\min}\approx 400\,\mu\mathrm{H}$. An example is shown in Fig. 9(a). The temporal behavior is distinctly different from that of the SLO. The frequency is again in the kHz range. However, for $V<200\,\mathrm{mV}$, it increases with increasing voltage [Fig. 9(b)]. Further, the frequency depends on the inductance.[2] This second type of oscillations can also be observed at temperatures

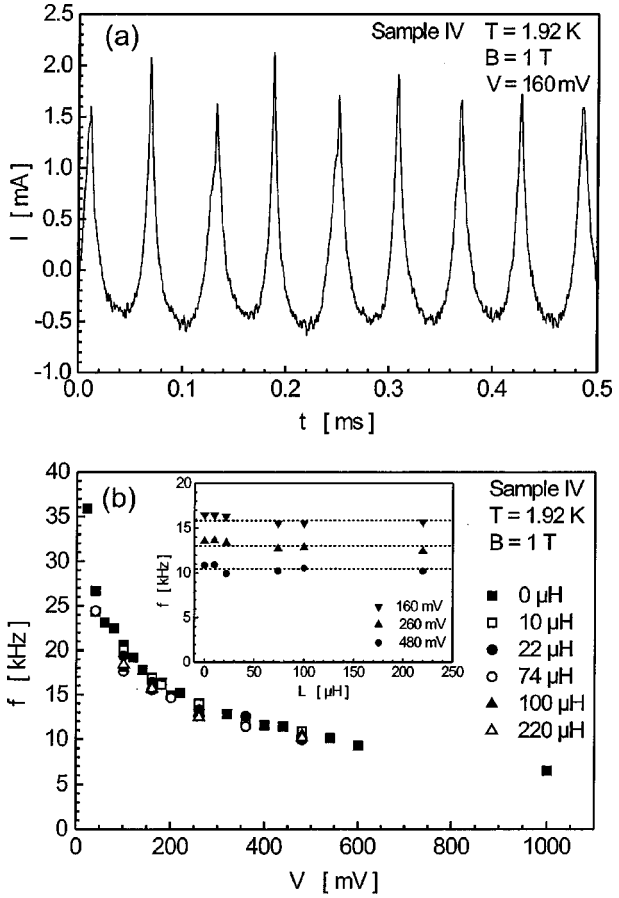

FIG. 8. (a) Oscillatory part of the current vs time at $T=1.92\,\mathrm{K}$, $B=1.00\,\mathrm{T}$, and dc voltage $V=160\,\mathrm{mV}$. A current offset has been subtracted. $L<L_{\min}=400\,\mu\mathrm{H}$. (b) Frequency f of the spontaneous oscillation vs the dc voltage V for different values of $L\leqslant 220\,\mu\mathrm{H}$ as indicated. $T=1.92\,\mathrm{K}$ and $B=1.00\,\mathrm{T}$. The inset indicates the independence of f upon L in the range $L\leqslant 220\,\mu\mathrm{H}$.

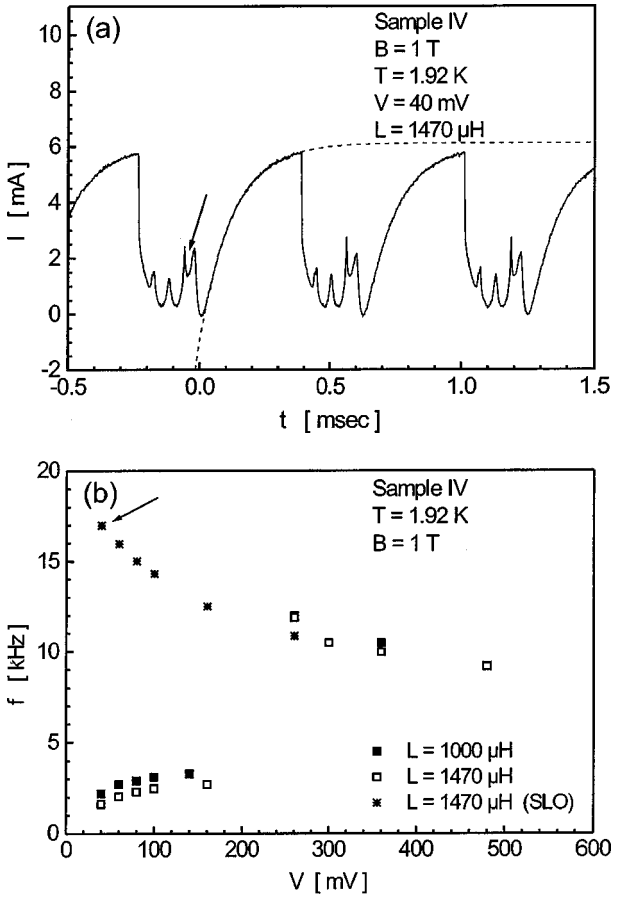

FIG. 9. (a) Oscillatory part of the current versus time at $T=1.92\,\mathrm{K}$, $B=1.00\,\mathrm{T}$, dc voltage $V=40\,\mathrm{mV}$, and $L=1470\,\mu\mathrm{H}$. A current offset has been subtracted. (b) Frequency f of the spontaneous oscillations vs the dc voltage V for two values of L as indicated. $T=1.92\,\mathrm{K}$ and $B=1.00\,\mathrm{T}$. At $V>200\,\mathrm{mV}$ the voltage dependence of f changes. The crosses indicate the higher-frequency component superimposed on the CLO mode and indicated by the arrows.

$T>2.17\,\mathrm{K}$. We refer to this type as circuit limited oscillations (CLO's).

At higher voltages at $T<2.17\,\mathrm{K}$ the temporal shape and frequency of the second type of oscillations changes to the SLO type. In the voltage dependence of the frequency in Fig. 9(b) this change can be seen for $V>200\,\mathrm{mV}$. In the low-voltage regime the CLO's are superimposed by another oscillation with higher frequency and small amplitude [Fig. 9(a)]. Plotting the higher frequencies in Fig. 9(b), we note qualitatively good agreement with the SLO behavior. Apparently, for $L>400\,\mu\mathrm{H}$ both types of oscillations are superimposed, with the CLO's dominating at $V<200\,\mathrm{mV}$. Our classification of the spontaneous resistance oscillations in the mixed state of NCCO in terms of SLO's and CLO's is similar to an earlier discussion of the dynamics of current filaments generated during avalanche breakdown in *p*-doped germanium.[17]

A. Circuit-limited oscillations

By definition, CLO's are oscillations generated by the interaction between the measuring circuit and the VIC of the sample. The mechanism deals with global features such as voltage, current, and resistance. It can be explained in terms of a simple model based on the circuit of Fig. 7 and the following arguments. In Fig. 10 the sequential steps during an oscillatory cycle are indicated schematically. For simplicity we have ignored the existence of a critical current due to flux-pinning. The low-Ohmic and high-Ohmic states of the S-shaped VIC are linearized by means of the two Ohmic resistances R_1 and R_2, respectively. Starting from the low-Ohmic state of R_1, by shifting the load line (dotted line) current and voltage of the VIC are increased along the branch with R_1. All stable points are located at the intercepts I_1 and I_2 of the load line with the branches of the states R_1 and R_2, respectively. If the current exceeds the maximum value I_t on the VIC, a transition to the higher Ohmic state of R_2 takes place. Following the abrupt switch from R_1 to R_2, a relaxation process toward the next stable current value I_2 sets in, which is dominated by the inductance L. Now L acts like a current source, effecting a ''quasi-current-controlled'' movement along the VIC with the typical exponential time dependence of an L-R circuit. At the current I_h another

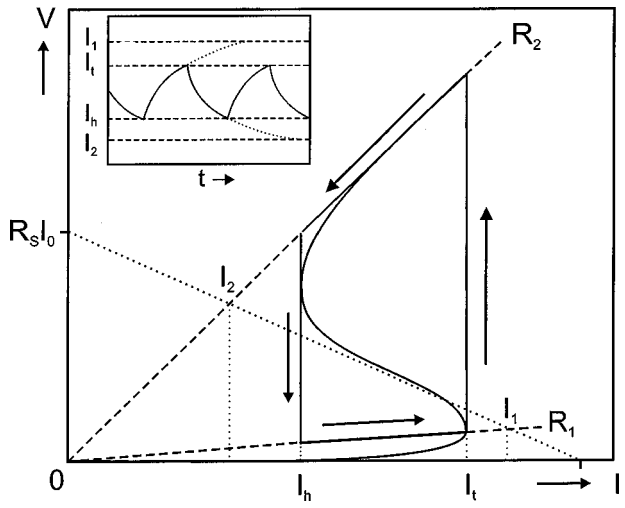

FIG. 10. S-shaped VIC and schematics of the sequential steps during a cycle of the CLO. The inset shows the time dependence of the current. Further details are given in the text.

switch from R_2 to R_1 occurs. The subsequent relaxation process toward the next stable fixed point I_1 ends at I_t, where the whole cycle starts again. The expected temporal current signal during this cycle is shown schematically in the inset of Fig. 10.

The relaxation times of the exponential time dependence of the relaxation process are proportional to L. Hence, the frequency of the CLO is expected to show the proportionality $f=A/L$, which is well confirmed by experiment.[2,18] A detailed analysis of the circuit of Fig. 7 using the given circuit parameters also yielded the correct magnitude of the proportionality constant A.[18]

From this mechanism we conclude that CLO's represent global oscillations of the sample, where localized dissipative structures do not play any role. This is also well confirmed by the spatially and temporally resolved flux-flow resistance measurements, as shown by the simultaneous recording of the time-dependent voltages in the three sample sections. A typical example is presented in Fig. 11, together with the oscillatory sample current. For clarity the oscillatory voltage curves are shifted by 220 mV relative to each other. The dc bias points were $V=54\,\mathrm{mV}$ and $I=60.7\,\mathrm{mA}$. During these measurements an external inductance of 1470 μH was added in series with the sample. The current indicated in the bottom trace shows the relaxation-type exponential behavior (see the inset of Fig. 10). The three voltage signals are seen to be exactly in phase. Furthermore, the maximum voltages are reached in the sample sections during the steeply decreasing part of the current oscillation. This part coincides with the fraction of the cycle in which the sample resides in the high-Ohmic state. During the increasing part of the current oscillation the voltage signal remains in the μV range and, hence, is not resolved in the recordings of Fig. 11. We conclude that Fig. 11 exactly shows the expected behavior. Finally, we note that the switching between the Low-ohmic and High-ohmic global states of the sample is sufficiently fast such that it does not show up in the form of an additional structure in the spatially and temporally resolved recordings of Fig. 11.

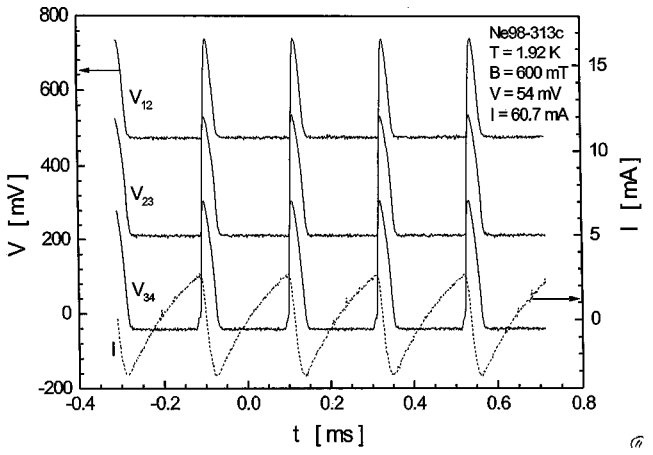

FIG. 11. Spatially resolved voltages V_{12}, V_{23}, and V_{34} (solid lines) and current I (dashed line, shifted vertically by an offset) vs time for a typical CLO mode. $T=1.92\,\mathrm{K}$, $B=600\,\mathrm{mT}$, dc voltage $V=54\,\mathrm{mV}$, the dc current is 60.7 mA, and $L=1470\,\mu\mathrm{H}$.

B. Structure-limited oscillations

SLO's appear to be generated by a local mechanism leading to spatiotemporal structures in the sample. Again, important clues are expected from the spatially resolved measurement of the time-dependent flux-flow voltage. A typical case is presented in Fig. 12, together with the oscillatory sample current. For clarity all oscillatory traces are shifted vertically, such that the vertical axes only yield the relative changes. The two vertical lines mark the phase of two subsequent current maxima. The dc bias points were $V=74\,\mathrm{mV}$ and $I=46\,\mathrm{mA}$. In contrast to the CLO's, there now exists a distinct phase difference between the three voltage oscillations. The phase of the voltage V_{12} is opposite to that of the two other voltages V_{23} and V_{34}. Depending on the experimental parameters, other configurations of the relative phases of the three voltages have also been observed.

From the time-averaged and spatially resolved measurements in Sec. III, we have concluded that with increasing

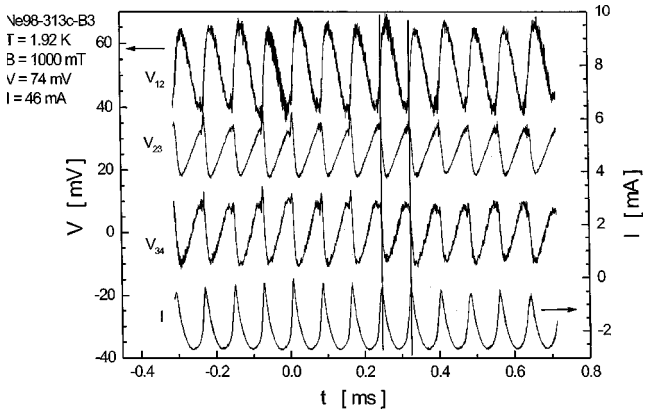

FIG. 12. Spatially resolved voltages V_{12}, V_{23}, and V_{34} (upper three traces as indicated) and current I (bottom trace) versus time for a typical SLO mode. All traces are shifted vertically by offsets, $T=1.92\,\mathrm{K}$, $B=1.00\,\mathrm{T}$, the dc voltage is 74 mV, and the dc current is 46 mA.

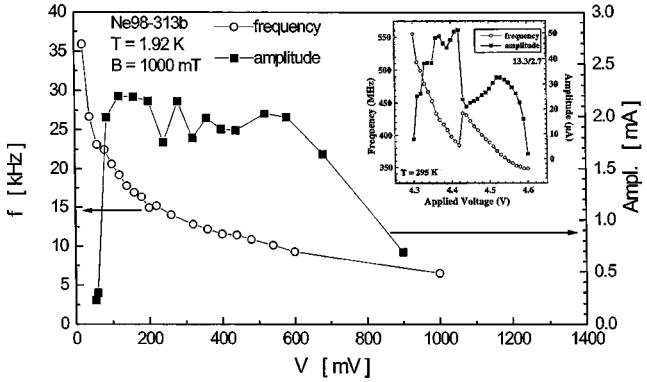

FIG. 13. Peak-to-peak amplitude (solid squares) and frequency (open circles) of the current oscillations vs the dc bias voltage for a typical case of SLO. $T=1.92\,\mathrm{K}$ and $B=1.00\,\mathrm{T}$. For comparison, the inset shows a similar plot of Ref. 19 for spontaneous resistance oscillations in a doped GaAs-AlAs semiconductor superlattice.

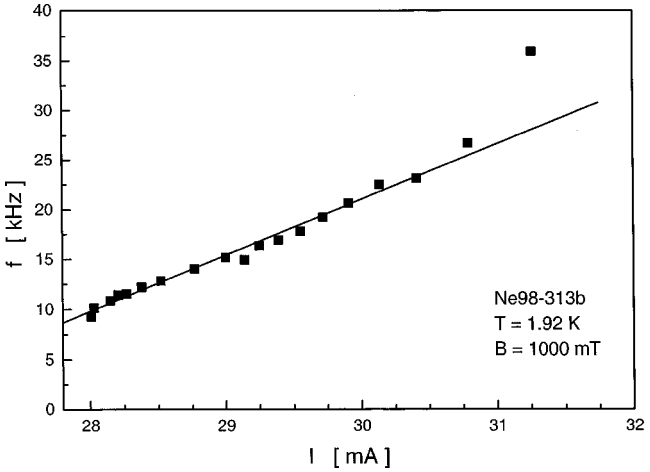

FIG. 14. Frequency data of Fig. 13 plotted vs the dc bias current.

voltage a single high-electric-field domain gradually expands from one end of the sample to the other. We interpret the spontaneous resistance oscillations in terms of a breathing movement of the domain boundary. The location of this domain boundary then determines the phase behavior of the three sample sections. However, keeping in mind that voltage V_{12} in particular can show maxima and minima as a function of current (see Fig. 3), the phase behavior of the voltage oscillations in the three sample sections can be quite complex. The breathing movement of the domain boundary associated with the spontaneous current oscillations apparently results in an increased noise level of the time-averaged measurements of the VIC's, if the domain boundary is located near the border between two sample sections (see Fig. 3, and its discussion in Sec. III). In this case the details of the measuring circuitry and electronics become important. A detailed study of these points is beyond the scope of this paper.

The dependence of the (peak to peak) amplitude and frequency of the current oscillations on the time-averaged bias voltage is shown in Fig. 13 for a typical case. The amplitude in the range 1–3 mA is small compared to the time-averaged current of 20–60 mA of the bias points on the VIC. At small voltages, upon the domain nucleation the amplitude strongly increases with the voltage, and then remains approximately constant. When the bias point leaves the NDR regime of the VIC, the amplitude decreases again. The amplitude of the voltage oscillations shows qualitatively the same behavior, with the maximum peak-to-peak amplitude of 10–20 mV being an order of magnitude smaller than the bias voltage. The relatively small amplitude of the oscillations supports our interpretation in terms of a breathing movement of the domain boundary. As we see from Fig. 13, the frequency decreases with increasing voltage.

The spontaneous oscillations we have observed in the flux-flow resistance of NCCO are highly similar to the resistance oscillations observed recently in doped GaAs-AlAs semiconductor superlattices.[19] For comparison, plots of the frequency and amplitude of these current oscillations as functions of the voltage are shown in the inset of Fig. 13. Except for the jump at about 4.4 V, the features are similar to our observations in NCCO. The oscillations in the semiconductor superlattice have been interpreted in terms of a breathing mode of a high-electric-field domain.[19]

Returning to the dependence of the oscillation frequency on the voltage shown in Figs. 8, 9, and 13, we note that, in the NDR regime, where these data were taken, the current decreases with increasing voltage. In Fig. 14 the frequency data of Fig. 13 are plotted versus the current. The frequency is seen to increase nearly linearly with the current. The straight line drawn through the points extrapolates to zero frequency at an offset current of about 26.5 mA. The development of a model for explaining this current dependence of the oscillation frequency needs further experimental and theoretical investigations.

V. SUMMARY AND CONCLUSIONS

The flux-flow resistance in epitaxial *c*-axis-oriented films of NCCO has been studied at 1.92 K, with the samples immersed in superfluid helium. Under quasi-voltage bias a branch with NDR appears in the VIC, suggesting a pronounced electric-field dependence of the flux-flow resistance. The extension of this NDR branch increases with decreasing magnetic field. Spatially resolved and time-averaged resistance measurements show that in the NDR regime of the VIC a single high-electric-field domain, nucleated on one end of the sample, with increasing voltage, grows from this end of the sample to the opposite end. This nucleation and growth process was found to be independent of the electric current direction. The generation of the high-electric-field domain is explained by a quasiparticle energy shift in the electric field, reaching a value near the energy gap where the quasiparticle DOS and, hence, the phase space available for scattering, strongly increase with energy. From this model the magnetic-field dependence of the hysteresis can also be understood.

Performing time-resolved resistance measurements in the NDR regime, two types of spontaneous oscillations are observed. The first type (CLO) is a global switching oscillation where the total sample oscillates between high-Ohmic and

low-Ohmic states. For this type to appear, an inductance L above a specific minimum value must be placed in series with the sample. The frequency f then shows the proportionality $f \sim L^{-1}$, and the current follows the typical relaxation behavior of a L-R circuit. The second type (SLO) is not affected by an external inductance below the minimum value mentioned above added to the circuit. It is interpreted in terms of a breathing movement of the domain boundary. In contrast to the CLO, in the SLO the individual voltage oscillations in the three sections show distinct phase differences. The phase behavior of the three sample sections is determined by the location of the domain boundary in the sample.

It appears to be the distinct energy dependence of the quasiparticle scattering rate which results in the highly nonlinear behavior of the flux-flow resistance and in the generation of spatiotemporal structures during the flux-flow process in NCCO. Since the symmetry of the pair wave function strongly affects the electronic structure of the quasiparticle system, the correct symmetry represents a crucial input of a model for explaining the observed electric-field dependence of the flux-flow resistance.

ACKNOWLEDGMENTS

Financial support of this work by the Deutsche Forschungsgemeinschaft is gratefully acknowledged. R.P.H. recieved support from the European Science Foundation (Program VORTEX).

[1] O. M. Stoll, S. Kaiser, R. P. Huebener, and M. Naito, Phys. Rev. Lett. **81**, 2994 (1998).
[2] O. M. Stoll, A. Wehner, R. P. Huebener, and M. Naito, Physica B **284-288**, 827 (2000).
[3] O. M. Stoll, R. P. Huebener, S. Kaiser, and M. Naito, J. Low Temp. Phys. **118**, 59 (2000).
[4] R. P. Huebener, S. Kaiser, and O. M. Stoll, Europhys. Lett. **44**, 772 (1998).
[5] D. H. Wu, J. Mao, S. N. Mao, J. L. Peng, X. X. Xi, T. Venkatesan, R. L. Greene, and S. M. Anlage, Phys. Rev. Lett. **70**, 85 (1993).
[6] S. M. Anlage, D. H. Wu, J. Mao, X. X. Xi, T. Venkatesan, J. L. Peng, and R. L. Greene, Phys. Rev. B **50**, 523 (1994).
[7] C. W. Schneider, Z. H. Barber, J. E. Evetts, S. N. Mao, X. X. Xi, and T. Venkatesan, Physica C **233**, 77 (1994).
[8] L. Alff, A. Beck, R. Gross, A. Marx, S. Kleefisch, Th. Bauch, A. Sato, M. Naito, and G. Koren, Phys. Rev. B **58**, 11 197 (1998).
[9] S. Kashiwaya, T. Ito, K. Oka, S. Ueno, H. Takashima, M. Koyanagi, Y. Tanaka, and K. Kajimura, Phys. Rev. B **57**, 8680 (1998).
[10] L. Alff, S. Meyer, S. Kleefisch, U. Schoop, A. Marx, A. Sato, M. Naito, and R. Gross, Phys. Rev. Lett. **83**, 2644 (1999).
[11] C. C. Tsuei and J. B. Kirtley, Phys. Rev. Lett. **85**, 182 (2000).
[12] J. O. Kokales, P. Fournier, L. V. Mercaldo, V. V. Talanov, R. L. Greene, and S. M. Anlage, Phys. Rev. Lett. **85**, 3696 (2000).
[13] O. M. Stoll, R. P. Huebener, S. Kaiser, and M. Naito, Phys. Rev. B **60**, 12 424 (1999).
[14] R. P. Huebener, O. M. Stoll, A. Wehner, and M. Naito, Physica C **332**, 187 (2000).
[15] R. P. Huebener, O. M. Stoll, A. Wehner, and M. Naito, Physica C **338**, 221 (2000).
[16] R. P. Huebener, O. M. Stoll, and S. Kaiser, Phys. Rev. B **59**, R3945 (1999).
[17] U. Rau, W. Clauss, A. Kittel, M. Lehr, M. Bayerbach, J. Parisi, J. Peinke, and R. P. Huebener, Phys. Rev. B **43**, 2255 (1991).
[18] O. M. Stoll, Ph.D. thesis, University of Tübingen, 2000.
[19] J. Kastrup, R. Hey, K. H. Ploog, H. T. Grahn, L. L. Bonilla, M. Kindelan, M. Moscoso, A. Wacker, and J. Galan, Phys. Rev. B **55**, 2476 (1997).